Met. Mater. Int., Vol. 20, No. 5 (2014), pp. 825~834
doi: 10.1007/s12540-014-5005-y

An Upper Bound Solution for Twist Extrusion Process

M. Seyed Salehi[1], N. Anjabin[2], and H. S. Kim[3,*]

[1]K. N. Toosi University of Technology, Department of Materials Science and Engineering, P.O. Box: 15875-4416, Tehran, Iran
[2]Shiraz University, School of Engineering, Department of Materials Science and Engineering, Zand Ave., Shiraz, Iran
[3]Pohang University of Science and Technology, Department of Materials Science and Engineering, Pohang 790-784, Korea

(received date: 14 August 2013 / accepted date: 27 December 2013)

Twist extrusion, a promising severe plastic deformation technique for grain refinement down to ultrafine/ nanocrystalline microstructures, was introduced as an attempt to provide large plastic deformation conditions similar to those in high pressure torsion while allowing large workpiece dimensions for industrial applications. As a relatively new severe plastic deformation technique, twist extrusion requires in-depth investigation of its plastic deformation characteristics. In this study, the twist extrusion process with a square shape die cavity has been analyzed using an upper bound solution to estimate the required power, deformation pattern, and optimum process condition. The analysis has been performed based on two kinematically admissible velocity fields while the effects of friction condition, die geometry, and mean equivalent strain have been considered. The results indicate that the die geometry and process parameters can dramatically change the deformation pattern and extrusion power.

Keywords: severe plastic deformation, twist extrusion, upper bound solution, grain refinement

1. INTRODUCTION

Ultrafine grained materials have been shown to have superior mechanical properties in comparison with conventional coarse-grained polycrystalline materials [1-4]. Severe plastic deformation (SPD) processing has been employed as an efficient route for the production of bulk ultrafine- and even nano-grained structures in metallic materials [5,6]. In this regard, various methods and techniques are utilized to refine the grain structure by applying large shear strains associated with high hydrostatic pressure, such as equal channel angular pressing (ECAP) [7-12], accumulative roll bonding (ARB) [13-15], high pressure torsion (HPT) [16-18], tubular channel angular pressing [19], caliber rolling [20], and twist extrusion (TE) [1,21-31].

In the TE process, a specimen with non-circular cross-section is extruded through a twisted die cavity while the original cross-section is preserved. In this method, the direction of material flow remains unchanged so extrusion die can be easily installed in conventional industrial lines. Also, the amount of wasted material in this method is lower than the other routine SPDs, e.g. ECAP [22]. In this method shearing plastic strain is applied to billet on surface perpendicular to the extrusion axis. To estimate the required power and deformation pattern during SPD processes several numerical and analytical methods such as the Finite Element Method (FE) [7,16,21,26] and Upper Bound (UB) theorem [27,32] have been employed. In some works, the results obtained from the FEM were used to validate the results of UB analysis of the SPD process [33,34]. Beygelzimer *et al.* [25] investigated the kinematics of metal flow during TE by reconstruction of experimental stream lines and by proposing a kinematically admissible velocity field which is closest to the experimental stream lines. Akbari Mousavi *et al.* [21] analyzed the TE of titanium alloys using an FE model which found the occurrence of maximum and minimum equivalent strains at the corner and the center of the extruded billet, respectively. Khoddam *et al.* [32] proposed an UB model to analyze the interaction between die and material and process pressure during axi-symmetric forward spiral extrusion. Seyed-Salehi and Serajzadeh [27] developed an UB solution in TE with elliptical die cross-section. They proposed a kinematically admissible velocity field which satisfies the velocity boundary conditions and mass conservation to investigate the flow pattern and the UB theorem used to calculate extrusion power for different die geometries and fric-

*Corresponding author: hskim@postech.ac.kr

tion conditions. They found that the ratio of length to diameter of die cavity (*i.e.* die aspect ratio), is an important factor to determine the flow pattern in TE process, and using inappropriate die aspect ratio may cause press plunger bending and increase in frictional force. Some researchers mixed TE with the other SPD approaches to develop more homogeneous strain distribution. Kocich *et al.* [35] and Raj *et al.* [26] combined ECAP and TE to investigate the effect of strain path on grain refinement and the equivalent strain distribution.

According to the published literature, it seems that further investigations are still needed to evaluate the effect of process parameters on the deformation mechanics during TE. In this work, the TE process of rectangular cross-sections is considered. An UB solution is proposed to predict the extrusion power, the optimum working conditions, and the minimum critical aspect ratio of the die regarding processing parameters such as equivalent strain, friction condition, and die geometry. In the first stage, the square-shaped die cavity is formulated using Fourier expansion and a second order polynomial function is introduced to determine the amount of twist angle as a function of distance from the die entry. Then, two kinematically admissible velocity fields are proposed and the UB theorem is utilized to estimate the required power for extrusion.

2. GENERAL FORMULATION OF EXTRUSION DIE SHAPE

The first step in the theoretical analysis of the TE process is determination of die cavity geometry. In order to propose a general formulation for the die geometry, an arbitrary die cross-section is assumed, as schematically shown in Fig. 1(b). In this figure, the origin of a cylindrical coordinate system (r, θ, z) is located at the center of the die entry and the z-axis coincides with the extrusion direction. The die cavity surface is expressed by the following Eq.

$$R = \Psi(\theta, z) \text{ where } \begin{cases} 0 \le \theta \le 2\pi \\ 0 \le z \le L \end{cases}, \tag{1}$$

where R is the radius of the die cavity which is defined as a function of "θ" and "z", and L is the die length. The die cavity profile at the entry region of die, i.e. $z = 0$, can be expressed as:

$$R|_{z=0} = \psi(\theta) \text{ where } 0 \le \theta \le 2\pi . \tag{2}$$

According to Fig. 1(b), by moving along the z-axis, the cross section is twisted as "γ" and accordingly, the following Eq can be written:

$$\tan\beta = \frac{dz}{R d\gamma}, \tag{3}$$

where β is the angle between moving direction in r-θ plane.

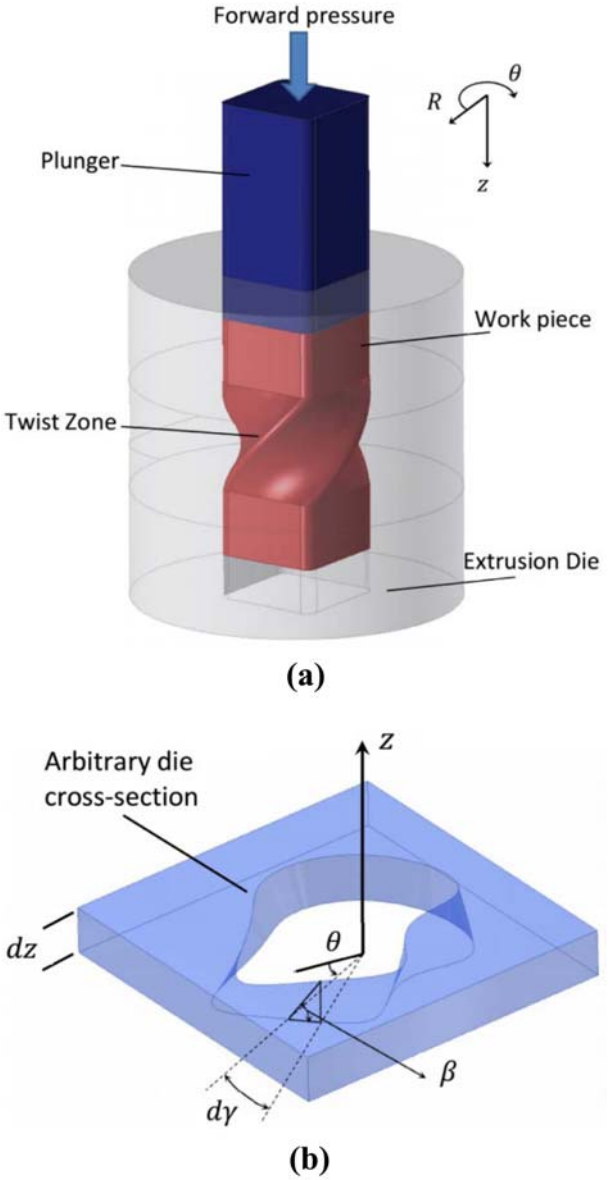

Fig. 1. (a) Schematic illustration of twist extrusion process and (b) extrusion die by arbitrary cross-section.

As the cross section of the die cavity must be invariable along the z-axis, thus, $d\gamma/dz$ should be solely a function of "z" as:

$$\frac{d\gamma}{dz} = f(z), \tag{4}$$

where $f(z)$ denotes twisting function. By employing a simple integration, the twist angle of the die cross-section at the "z" position may be determined as follows.

$$\gamma(z) = \int_0^z f(\xi) d\xi . \tag{5}$$

Hence, the die cavity surface in the TE die may be expressed by

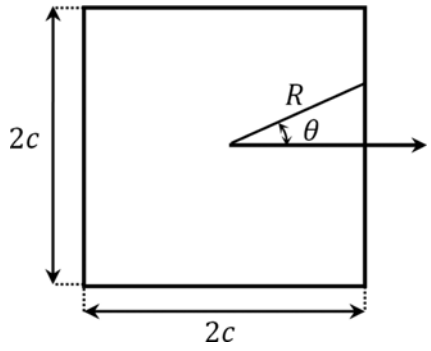

Fig. 2. Square shape cross-section of TE die cavity.

the following general Eq.

$$\Psi(\theta, z) = \psi(\theta - \gamma(z)) . \tag{6}$$

Therefore, the operational zone of the extrusion die cavity can be introduced by the following general Eq in cylindrical coordinate system.

$$R = \psi\left(\theta - \int_0^z f(\xi) d\xi\right) . \tag{7}$$

In this study, the TE of a billet with square cross-section has been studied. Figure 2 shows a square cross-section for die cavity in polar coordinate. The following periodic Eq describes a square with side length 2c.

$$\begin{cases} \psi(\theta) = c \sec(\theta) & \text{where } -\pi/4 \le \theta \le \pi/4 \\ \psi(\theta + n\pi/2) = \psi(\theta) \end{cases} . \tag{8}$$

Here $\psi(\theta)$ is a continuous periodic function and can be expressed by Fourier series expansion into the summation of a set of simple oscillating functions. Since $\psi(\theta)$ is an even periodic function, it can be expanded by cosine Fourier expansion as follows:

$$\psi(\theta) = a_0 + \sum_{n=1}^{N} a_n \cos(4n\theta) , \tag{9}$$

where a_0 and a_n are the expansion coefficients.

$$a_0 = \frac{4}{\pi} \int_0^{\frac{\pi}{4}} \psi(\theta) d\theta , \tag{10}$$

$$a_n = \frac{8}{\pi} \int_0^{\frac{\pi}{4}} \psi(\theta) \cos(4n\theta) d\theta .$$

Substituting Eq. (9) in Eq. (7) results in the following Eq.

$$R = a_0 + \sum_{n=1}^{N} a_n \cos\left(4n\left(\theta - \int_0^z f(\xi) d\xi\right)\right) . \tag{11}$$

In fact, Eq. (11) describes the internal surface of the TE die cavity at different positions.

3. UPPER BOUND SOLUTION

According to the UB theorem, among all kinematically admissible velocity fields, the actual one minimizes the power expressed by the following Eq (12):

$$\boldsymbol{J}^* = 2k \int_\Omega \left(\frac{1}{2} \dot{\varepsilon}_{ij} \dot{\varepsilon}_{ij}\right)^{\frac{1}{2}} d\Omega + \sum_i \int_{\Gamma_s^i} k \left|\Delta V_{\Gamma_s^i}\right| d\Gamma + \sum_i \int_{\Gamma_f^i} T_i \left|\Delta V_{\Gamma_f^i}\right| d\Gamma \tag{12}$$

where $\mathbf{J}^*$ is externally supplied power, "k" is shear yield stress and $\dot{\varepsilon}_{ij}$ is the kinematically admissible strain rate field. The first term in Eq. (12) determines the power dissipation due to internal plastic deformation over a deforming volume "Ω", the second term is the power losses with regards to velocity discontinuities "ΩV_{Γ_s}" on internal shearing surfaces "Γ_s", and the last term is the frictional power dissipation on the external interaction surfaces "Γ_f" with frictional traction "T" and interaction relative velocity "ΔV_{Γ_f}". The kinematically admissible strain rate field is derived from a kinematically admissible velocity field which satisfies the external boundary conditions as well as the mass conservation.

The cross section of deforming material remains unchanged throughout the TE process. It is assumed that each axial slice of material during the extrusion rotates along the "z" axis in a way that it satisfies the boundary condition (Fig. 3). The angular velocity "ω" of an axial slice of material along the "z" axis is proposed by the following Eq.

$$\omega = \frac{d\gamma}{dt} = \frac{d\gamma}{dz}\frac{dz}{dt} = v_z f(z) , \tag{13}$$

where v_z is the axial velocity component in the cylindrical

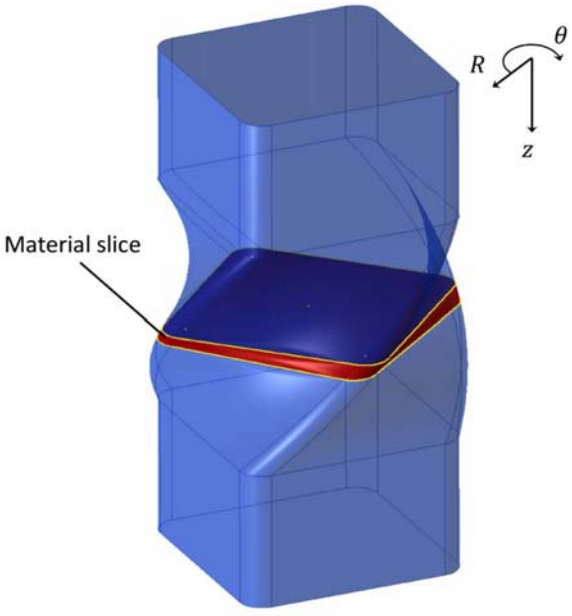

Fig. 3. Rotation of material slices with die surface cavity.

coordinate system. The constancy of the surface area of each axial slice and the principle of mass conservation confirm the steadiness of velocity component along the z-axis "v_z". Therefore, v_z is equal to the plunger velocity "v_0". The velocity component of the material in the θ direction is derived as follows.

$$v_\theta = r\omega = rv_0 f(z)\,. \tag{14}$$

Accordingly, the velocity component in radial direction "v_r" must be zero. Finally, regarding the above discussion and the experimental observations, two possible velocity fields are proposed. In the first one, a rigid cylindrical region within the deforming metal is assumed to be formed as displayed in Fig. 4, so the velocity field may be described as below:

$$V_i:\begin{cases} v_r = 0 \\ v_z = v_0 \\ v_\theta = \begin{cases} 0 & r \le \rho_1(\text{ZoneI}) \\ rv_0 f(z) & r > \rho_1(\text{ZoneII}) \end{cases} \end{cases}, \tag{15}$$

where ρ_1 is the radius of the rigid core which may vary between 0 and "c", i.e. half square side. Note that ρ_1 is the degree of freedom of the first velocity field that should be optimized. Furthermore, the second velocity field is introduced as:

$$V_{ii}:\begin{cases} v_r = 0 \\ v_z = \begin{cases} 0 & r > c \\ v_0 & r \le c \end{cases} \\ v_\theta = 0 \end{cases}. \tag{16}$$

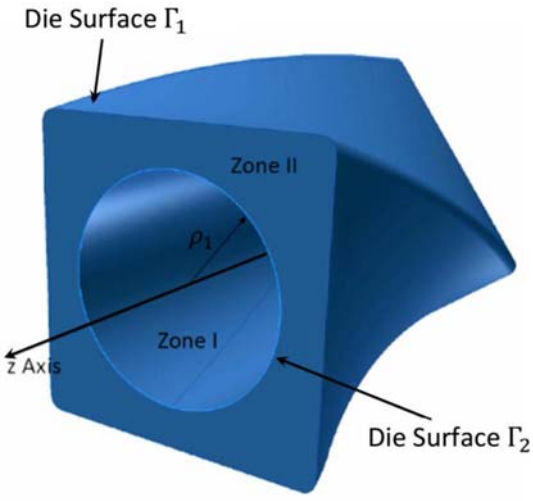

Fig. 4. Different zone in TE die according to the first velocity field.

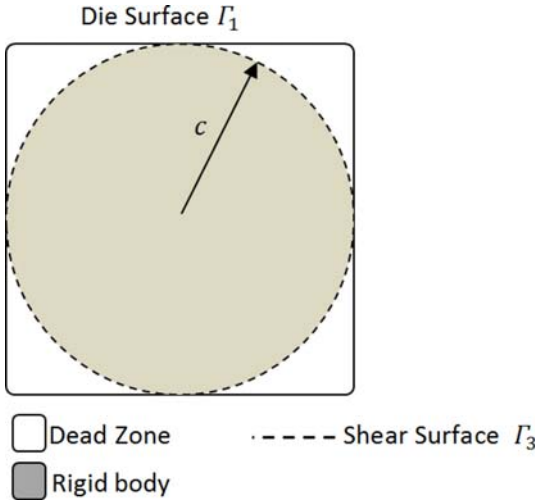

Fig. 5. Different zone in TE die according to second proposed velocity field.

In this situation, the surface zone and the die cavity interlock each other and a dead metal zone is created between the central zone and the die surface. The core of the billet passes through the extrusion channel without any deformation as shown in Fig. 5. Based on the first proposed velocity field, the kinematically admissible strain rate field can be introduced as below

$$\dot{\varepsilon}_{\theta z} = \frac{1}{2}\left(\frac{\partial v_\theta}{\partial_z} + \frac{1}{r}\frac{\partial v_z}{\partial \theta}\right) = \frac{1}{2} r v_0 f'(z)\,, \tag{17}$$

$$\dot{\varepsilon}_r = \dot{\varepsilon}_\theta = \dot{\varepsilon}_z = \dot{\varepsilon}_{rz} = \dot{\varepsilon}_{r\theta} = 0\,.$$

The externally supplied power ($\boldsymbol{J}^*$) for the proposed velocity fields are evaluated as a summation of internal power of plastic deformation, frictional power loses and the power dissipation due to velocity discontinuities. Internal power of plastic deformation, $\dot{w}_i$ may be calculated as:

$$\dot{w}_i = 2k\int_\Omega \left(\frac{1}{2}\dot{\varepsilon}_{ij}\dot{\varepsilon}_{ij}\right)^{\frac{1}{2}} d\Omega = \frac{kv_0}{\sqrt{2}}\int_0^L\int_0^{2\pi}\int_{\rho_1}^R |f'(z)| r^2 dr d\theta dz\,, \tag{18}$$

$$\dot{w}_i = \frac{kv_0}{3\sqrt{2}}\int_0^L\int_0^{2\pi} |f'(z)|(R^3(\theta,z) - \rho_1^3) d\theta dz\,. \tag{19}$$

The frictional power losses can be obtained by integration over the surface Γ:

$$\dot{w}_f = \int_\Gamma mk|\Delta V_\Gamma| d\Gamma\,, \tag{20}$$

where "m" is friction factor and ΔV_Γ velocity difference between the rigid die surface and the deforming material.

$$\Delta V_\Gamma = (v_\theta^2 + v_z^2)^{\frac{1}{2}} = v_0(1 + R^2(\theta,z) f^2(z))^{\frac{1}{2}}\,. \tag{21}$$

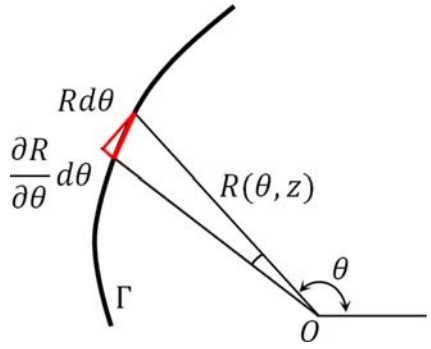

Fig. 6. Geometrical representation of die surface element.

Considering Fig. 6, $d\Gamma$ may be expressed as,

$$d\Gamma = \left[R^2(\theta,z)+\left(\frac{\partial R(\theta,z)}{\partial\theta}\right)^2\right]^{\frac{1}{2}} d\theta dz\,. \tag{22}$$

On the internal shear surface, Γ_1, the corresponding power is as:

$$\dot{w}_{s,\Gamma_1} = \int_{\Gamma_1} k|\Delta V_{\Gamma_1}|d\Gamma = k\rho_1\int_0^L\int_0^{2\pi}|\Delta V_{\Gamma_1}|d\theta dz$$

$$= 2\pi v_0 k\rho_1^2\int_0^L|f(z)|dz \tag{23}$$

Then, the required extrusion pressure for the first proposed velocity field "P_I" is determined:

$$\boldsymbol{J}_{\boldsymbol{I}}^{*} = 4c^2 v_0 P_I\,. \tag{24}$$

Hence, the relative extrusion pressure for the first velocity field can be written as:

$$\overline{P_I} = \frac{P_I}{\overline{\sigma}} = \frac{\dot{w}_i+\dot{w}_f+\dot{w}_{s,\Gamma_1}}{4\sqrt{3}c^2 k v_0}\,. \tag{25}$$

For the second proposed velocity field, $\dot{w}_i$ and $\dot{w}_f$ components of total dissipation power are equal to zero, and $\dot{w}_s$ can be determined using the following Eq.

$$\dot{w}_{s,\Gamma_2} = \int_{\Gamma_2} k|\Delta V_{\Gamma_2}|d\Gamma = \int_0^L\int_0^{2\pi} kc|\Delta V_{\Gamma_2}|d\theta dz = 8v_0 kcL\,. \tag{26}$$

Hence, relative extrusion pressure in this case is determined as below

$$\overline{P_{II}} = \frac{P_{II}}{\overline{\sigma}} = \frac{2L}{\sqrt{3}c}\,. \tag{27}$$

To obtain the optimal velocity field and extrusion pressure during the TE, $\overline{P_I}$ is minimized with respect to internal rigid radius "ρ_1" for the first proposed velocity field. Calculated $\overline{P_I}$ and $\overline{P_{II}}$ are compared with each other to characterize the optimal velocity field with the minimum externally supplied power.

4. TWISTING FUNCTION

The frictional, internal, and shear power losses are functions of twisting function, $f(z)$, and the change of twisting function affects the stable velocity field and the extrusion force. In this study, twisting function was assumed to be a second order polynomial function.

$$f(z) = b_1 z^2 + b_2 z + b_3\,, \tag{28}$$

where b_i are polynomial coefficients. At the entry and exit regions of the operational zone of the die, the material movement should be smooth, which should be considered in the definition of the twisting function. Therefore, β must be equal to $\pi/2$ at the entry ($z = 0$) and exit ($z = L$) sections. Therefore, the boundary conditions at entry and exit regions are derived as below.

$$f(0) = f(L) = 0\,. \tag{29}$$

The twisting function may be express as the following function to satisfy the boundary conditions.

$$f(z) = b_1 z(z-L)\,. \tag{30}$$

The TE die applies significant mean strain ($\bar{\varepsilon}_0$) to the billet during the process. The equivalent mean strain at a given radius can be obtained as:

$$\bar{\varepsilon}_0 = \frac{c}{\sqrt{6}}\int_0^L|f'(z)|dz\,, \tag{31}$$

where

$$|f'(z)|:\begin{cases} 2b_1\left(z-\dfrac{L}{2}\right) & \text{if} \quad z>L/2 \\ -2b_1\left(z-\dfrac{L}{2}\right) & \text{if} \quad z<L/2 \end{cases}. \tag{32}$$

So, Eq. (31) becomes

$$\bar{\varepsilon}_0 = \frac{c}{\sqrt{6}}\left(\int_0^{L/2}|f'(z)|dz+\int_{L/2}^L|f'(z)|dz\right) = \frac{b_1 L^2 c}{2\sqrt{6}}\,. \tag{33}$$

Then, the twisting function can be expressed as a function of equivalent mean strain:

$$f(z) = \frac{-2\sqrt{6}\bar{\varepsilon}_0}{cl^2}z(z-L)\,. \tag{34}$$

5. RESULTS AND DISCUSSION

As noted earlier, the die cavity of TE with square cross-section was expressed by a Fourier series expansion. The

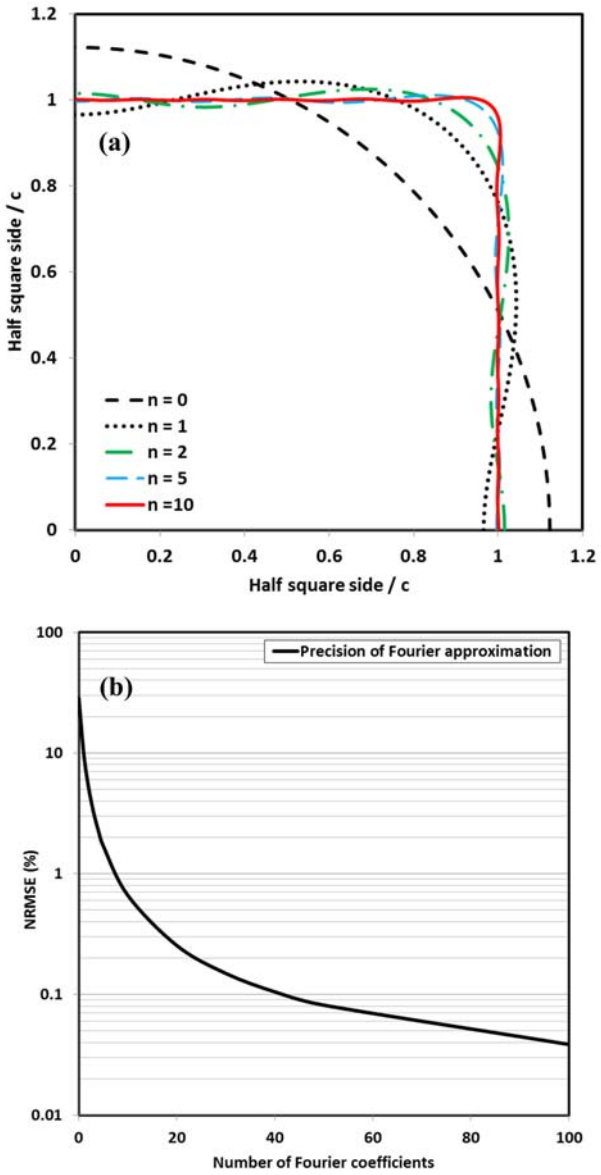

Fig. 7. (a) quarter of die cross-section obtained from Eq. (11) with different number of series term and (b) NRMSE of Fourier series approximation and exact value of square profile.

number of Fourier coefficients plays a prominent role in the precision of the die shape. Figure 7 shows the effect of an increasing number of series terms on the square profile approximation. Figure 7(a) illustrates a quarter of die cross-section with various number of Fourier coefficients. It is clear that increase of N in Eq. (11) enhances the precision of the die cavity approximation. To measure the correctness of the Fourier approximation the normalized root mean square error (NRMSE) of the estimated die cavity radius and the exact die radius was calculated. As shown in Fig. 7(b), a good approximation for square profile can be obtained using the first 30 terms of the Fourier series used in this study. Accordingly, the estimated die cavity surface with 30 Fourier coefficients and 50 degree

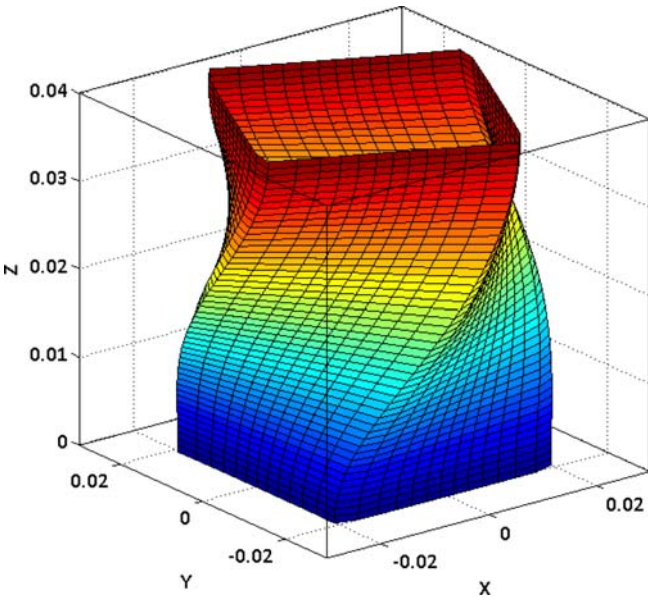

Fig. 8. Schematic illustration of twist extrusion die cavity with square cross-section.

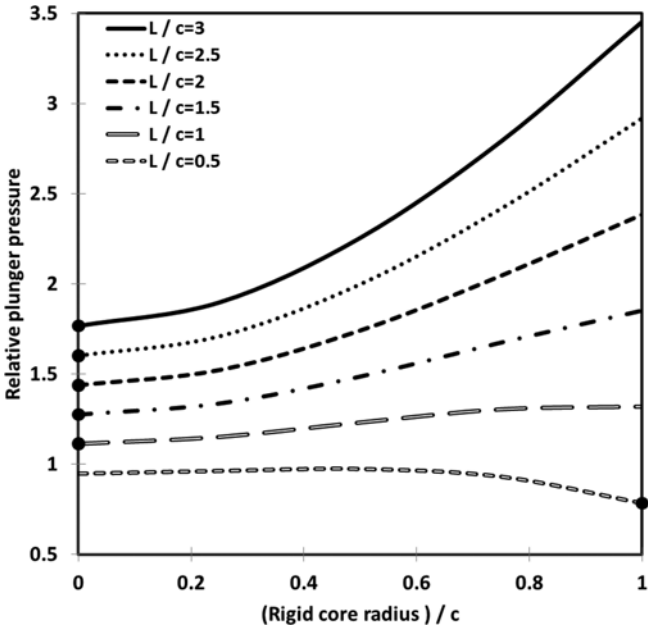

Fig. 9. The effect of rigid core radius on calculated relative plunger pressure for extrusion die with $\bar{\varepsilon}$=1, m=0.2.

twist is shown in Fig. 8.

The first velocity field has one degree of freedom "ρ_1" and a change in this parameter varies the dissipation of power during the process. The effect of rigid core radius on the relative plunger pressure ($\overline{P_l}$) for different die aspect ratios are shown in Fig. 9, where the mean equivalent applied mean strain and friction factor were taken to be constants ($\bar{\varepsilon}$ =1,m = 0.2). As expected, ρ_1 affects the internal and shearing power losses. Increasing ρ_1 increases the amount of shearing power and

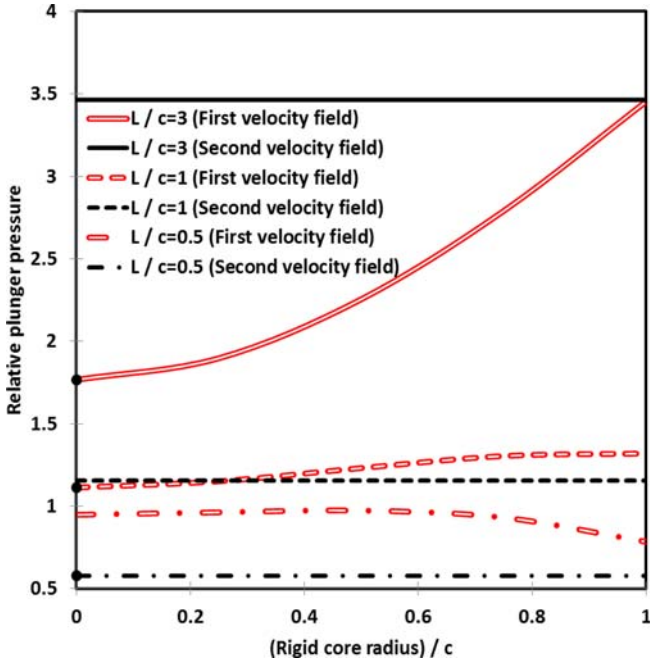

Fig. 10. Variation of relative plunger pressure with change in rigid core radius for different die lengths and velocity fields ($\bar{\varepsilon}$=1, m=0.2).

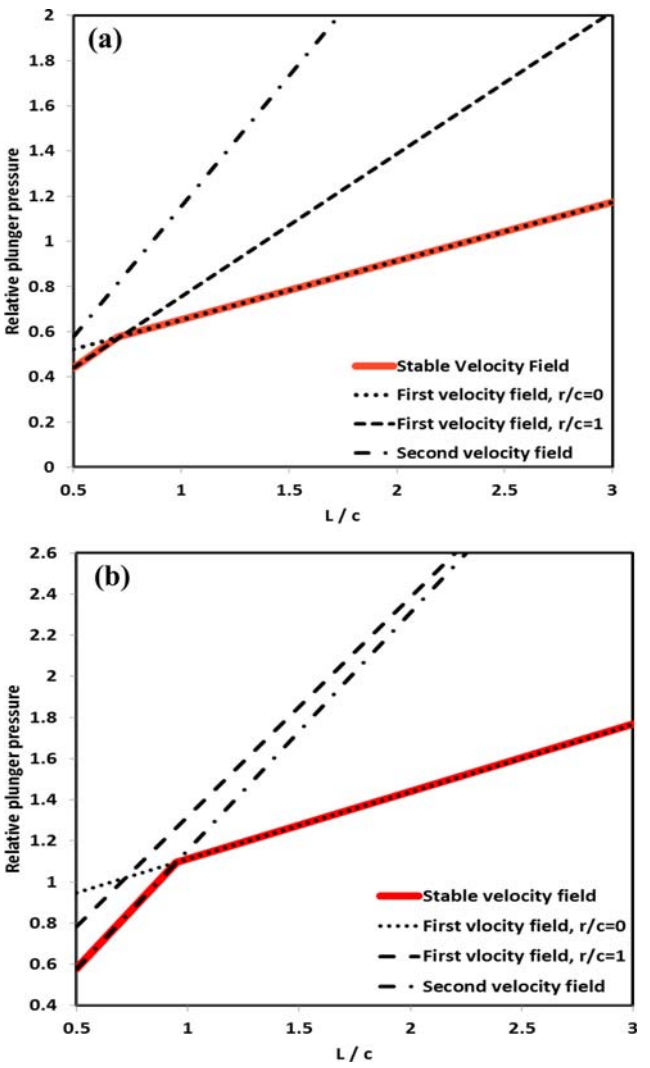

Fig. 11. the effect of aspect ratio on the relative plunger pressure, (a) $\bar{\varepsilon}$=0.5, m=0.2, (b) $\bar{\varepsilon}$=1, m=0.2.

decreases the amount of internal power. As depicted in Fig. 9, the minimum value of the extrusion power losses takes place at either $\rho_1 = 0$ or $\rho_1 = c$, depending on the die aspect ratio. With raising the die aspect ratio, the velocity field will be changed from the first proposed one with $\rho_1 = c$ to that of $\rho_1 = 0$. The effect of die aspect ratio on the relative plunger pressure for two proposed velocity fields are compared in Fig. 10. According to this figure, for the long dies, i.e. dies with high aspect ratio, V_i with $\rho_1 = 0$ controls the material flow and almost all the volume of the billet deforms during TE. In TE dies with a lower aspect ratio, the second velocity field governs the deformation regime and the billet sticks in die cavity.

Figure 11 depicts the relative plunger pressure vs. die aspect ratio at given equivalent mean strains of 0.5 and 1 where the friction factor was assumed to be $m = 0.2$. In this figure, the stable velocity field with the lowest dissipation power (relative plunger pressure) is illustrated by the solid line. For lower stain case (e=0.5) the first velocity fields with $\rho_1 = c$ and $\rho_1 = 0$ are governing fields for low and high die aspect ratios, respectively (Fig. 11(a)). As shown in Fig. 11(b), in the higher strain case, the first velocity field is stable for the die with high aspect ratio and the second velocity field is stable for the low aspect ratio. Therefore, depending on the amount of equivalent mean strain and die aspect ratio, there are two critical die lengths, where the strain distribution is changed significantly.

The first critical die aspect ratio (l_{c1}) occurs when the velocity field changes from first one with $\rho_1 = c$ to that of $\rho_1 = 0$ (see Fig. 11(a)). It can be easily found that l_{c1} is equal to $\sqrt{2}c/2$, which is independent of the equivalent mean strain or friction condition. The stable velocity field is shown in Fig. 12 for equivalent mean strain 0.5 and various friction factors. In this figure the bright and the dark regions denote the stable region of the first velocity field with or without rigid core, respectively. The other critical die length (l_{c2}), in which the velocity field changed from first velocity field to the second one, strongly depends on the friction condition. Its dependency is well illustrated in Fig. 13 with applied equivalent mean strain 1.0. It is observed that l_{c2} rises by increasing the friction factor. It is reasonable, because friction factor directly affects the frictional contribution power and increases the plunger pressure.

In addition to the die aspect ratio, the twist angle of die is also an important geometry parameter in determining the material flow pattern. Based on Eqs. 3, 4 and 34 by changing the twist angle of die with a given aspect ratio, the applied

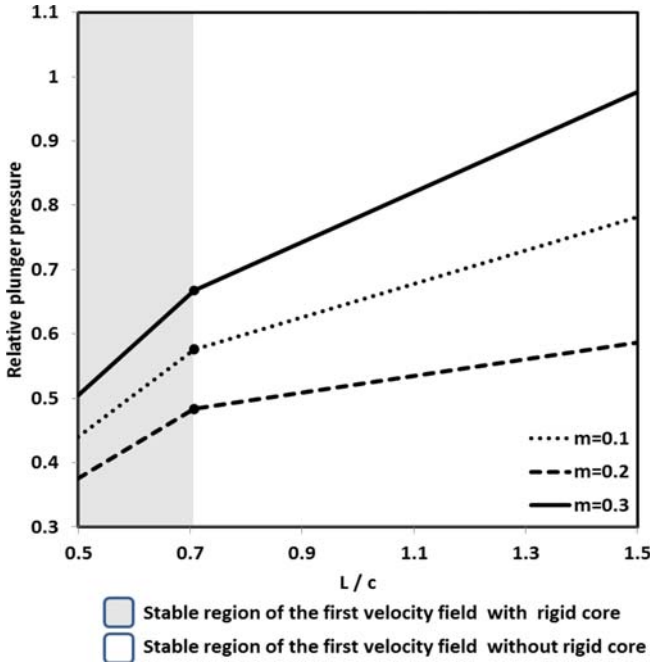

Fig. 12. The effect of friction on relative plunger pressure ($\bar{\varepsilon}$=0.5).

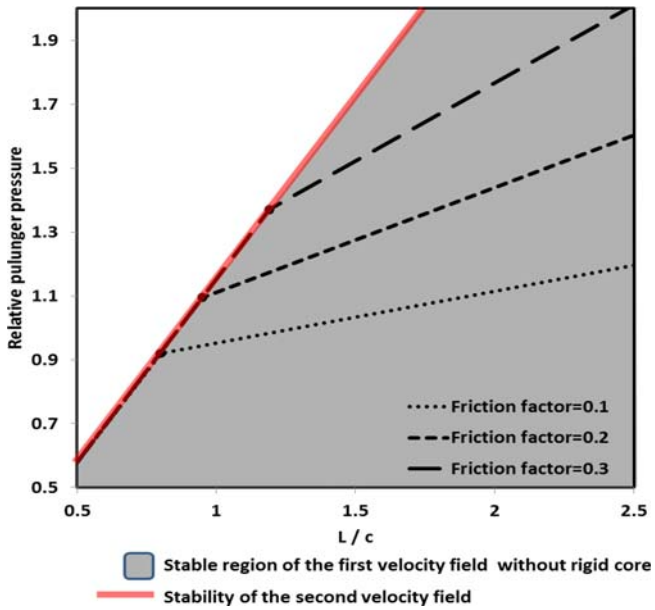

Fig. 13. The effect of friction on relative plunger pressure and critical die length ($\bar{\varepsilon}$=1).

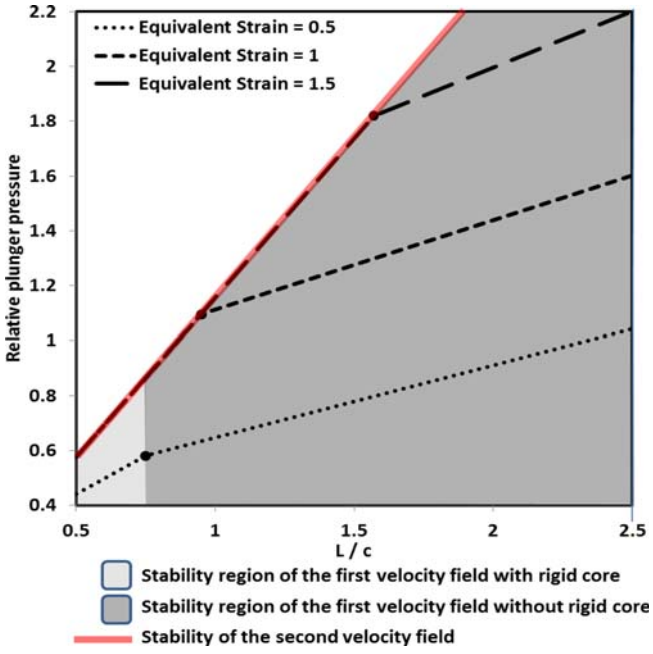

Fig. 14. The effect of equivalent strain on relative plunger pressure and critical die length ($\bar{\varepsilon}$=0.2).

mean strain is changed. Figure 14 demonstrates the stable regions of velocity fields as a function of applied effective mean strain. As shown in this figure, at low mean effective strain (i.e. $\bar{\varepsilon}_0 = 0.5$), for all the die lengths considered here, (i.e. $L = 0.5c$ to c), the first proposed velocity field is stable. Under this condition, the contribution of the internal energy in total power is lower than the other terms, but by increasing the amount of effective mean strain, from 0.5 to 1 and 1.5, at short die length the second velocity field will be stable. Also, the critical die length (l_{c2}) is increased while enhancing the effective strain. In total, the TE process in dies with small aspect ratio leads to strain concentration on the surface region of the billet in which the first velocity field with $\rho_1 = c$ is stable. An increase in die aspect ratio changes the strain distribution is changed and the rigid core is eliminated, i.e. stability of the first velocity field with $\rho_1 = 0$. In all TE dies, the first velocity field is changed to the second one by increasing the friction factor or twist angle, which results in material locking during TE. In this condition, the corners of the billet are locked in the TE die and the core moves through the stuck corners without any deformation as a rigid body. Figure 15 shows the locked corners and the rigid core in a die with the aspect ratio of 0.96. This result is for a commercially pure aluminum bar during the experimental TE process at room temperature. As shown in Fig. 15(a), the corner of the material gets stuck in the die and the core passes through the die without deformation. As a result, the cross-section of material after extrusion is circular which is shown in Fig. 15(b). This pattern is the same as the second velocity field of the proposed UB model which shows the accuracy of the model to predict the flow pattern.

Finally, in order to evaluate the extrusion power predicted by the present model, a comparison was made between results of the present model and predictions using a FE solution. To do so, a commercial FE package, DEFORM3D, was employed to investigate the material flow and plunger force during TE in which a rigid-plastic material with 300 MPa flow stress

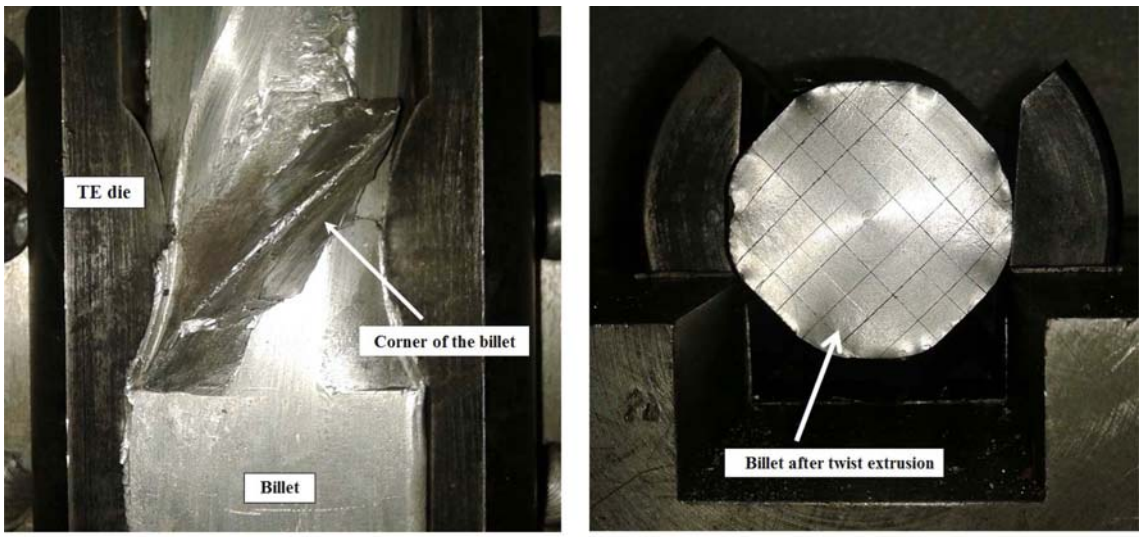

Fig. 15. Material flow during TE process in open die (a) side view of material and die (b) exit view of die.

Table 1. Comparison of relative plunger pressure between FEM and UB results for extrusion die with $\bar{\varepsilon} = 1$ and $m = 0.2$

Die aspect ratio	Relative plunger pressure	
	FEM results	UB results
0.7	0.78	0.8078
1.5	1.167	1.275
2	1.27	1.4378
3	1.56	1.7663

was modeled using 54450 linear tetrahedral elements with automatic remeshing. Also, in this model the 11885 nodes with 3 degrees of freedom at each node were used. Table 1 compares the two sets of data. As can be seen, there is a reasonable consistency between these results, which illustrates the validity of the employed UB solution.

6. CONCLUSIONS

In the present study, an upper bound model has been proposed to estimate the required power, optimum process condition, and die geometry in TE. The power predicted by the model was in reasonable agreement with the results of the FE analysis calculated using DEFORM3D. The results show that to achieve a relatively uniform strain distribution, the friction should be kept as low as possible, also, the die length should not be shorter than a critical value, *i.e.* $\sqrt{2}c/2$. If the die length is shorter than the critical value, inappropriate velocity fields, *i.e.* velocity fields with a central rigid zone, will be stable. If the die length is very long, the required power for extrusion increases significantly. Thus, the optimal die length should be selected a little longer than the critical die length.

ACKNOWLEDGEMENTS

This work was supported by the grant from the Ukraine–Korea joint research project (2001-0019214) funded by the National Research Foundation, Korea.

REFERENCES

1. D. Orlov, Y. Beygelzimer, S. Synkov, V. Varyukhin, N. Tsuji, and Z. Horita, *Mater. Sci. Eng. A* **519**, 105 (2009).
2. S.-S. Shin, K.-M. Lim, E.-S. Kim, and J.-C. Lee, *Korean J. Met. Mater.* **50**, 293 (2012).
3. T. E. Kim, S. W. Sohn, J. M. Park, C. W. Bang, W. T. Kim, and D. H. Kim, *Met. Mater. Int.* **19**, 667 (2013).
4. W. Wang, Y. Song, D. Gao, E. Y. Yoon, D. J. Lee, C. S. Lee, and H. S. Kim, *Met. Mater. Int.* **19**, 1021 (2013).
5. R. Z. Valiev, Y. Estrin, Z. Horita, T. G. Langdon, M. J. Zechetbauer, and Y. T. Zhu, *JOM* **58**, 33 (2006).
6. R. Haghayeghi, *Met. Mater. Int.* **18**, 777 (2012).
7. H. S. Kim, S.-H. Joo, and H. J. Jeong, *Korean J. Met. Mater.* **52**, 87 (2014).
8. I. H. Lee, S. I. Hong,and K. H. Lee, *Korean J. Met. Mater.* **50**, 931 (2012).
9. K. H. Lee and S. I. Hong, *Korean J. Met. Mater.* **51**, 621 (2013).
10. J.-J. Park, *Met. Mater. Int*. **18**, 439 (2012).
11. H. S. Kim, *Mater. Trans.* **42**, 536 (2001).
12. H. S. Kim and Y. Estrin, *Mater. Sci. Eng. A* **410**, 285 (2005).
13. S.-H. Lee and J.-H. Kim, *Korean J. Met. Mater.* **51**, 251 (2013).
14. C. H. Jeon, S. W. Han, B. D. Joo, C. J. Van Tyne, and Y. H. Moon, *Met. Mater. Int.* **19**, 1069 (2013).
15. Y. Saito, H. Utsunomiya, N. Tsuji, and T. Sakai, *Acta Mater.* **47**, 579 (1999).

16. Y. Song, W. Wang, D. Gao, E. Y. Yoon, D. J. Lee, and H. S. Kim, *Met. Mater. Inter.* **20**, 445 (2014).
17. E. Y. Yoon, D. J. Lee, B. Park, M. R. Akbarpour, M. Farvizi, and H. S. Kim, *Met. Mater. Int.* **19**, 917 (2013).
18. S. C. Yoon, Z. Horita, and H. S. Kim, *J. Mater. Proc. Tech*. **201**, 32 (2008).
19. G. Faraji, M. M. Mashhadi, and H. S. Kim, *Mater. Lett*. **65**, 3009 (2011).
20. T. Lee, C. H. Park, S.-Y. Lee, I.-H. Son, D.-L. Lee, and C. S. Lee, *Met. Mater. Int.* **18**, 391 (2012).
21. S. Akbari Mousavi, A. Shahab, and M. Mastoori, *Mater. Des.* **29**, 1316 (2008).
22. Y. Beygelzimer, D. Orlov, A. Korshunov, S. Synkov, V. Varyukhin, I. Vedernikova, A. Reshetov, A. Synkov, L. Polyakov, and I. Korotchenkova, *Solid State Pheno.* **114**, 69 (2006).
23. Y. Beygelzimer, D. Prilepo, R. Kulagin, V. Grishaev, O. Abramova, V. Varyukhin, and M. Kulakov, *J. Mater. Proc. Tech.* **211**, 522 (2011).
24. Y. Beygelzimer, O. Prokof'eva, and V. Varyukhin, *Russ. Metall. (Metally)* **2006**, 25 (2006).
25. Y. Beygelzimer, A. Reshetov, S. Synkov, O. Prokof'eva, and R. Kulagin, *J. Mater. Proc. Techn.* **209**, 3650 (2009).
26. K. H. Raj, R. S. Sharma, A. Sahai, and S. S. Sharma, *AIP Conference Proceedings*, p.507, AIP Publishing, Paris (2011).
27. M. Seyed Salehi and S. Serajzadeh, *Proc. Inst. Mech. Eng. Part C: J. Mech. Eng. Sci.* **223**, 1975 (2009).
28. M. I. Latypov, I. V. Alexandrov, Y. E. Beygelzimer, S. Lee, and H. S. Kim, *Comp. Mater. Sci.* **60**, 194 (2012).
29. R. Kulagin, M. Latypov, H. S. Kim, V. Varukhin, and Y. Beygelzimer, *Metall. Mater. Trans*. **44A**, 3211 (2013).
30. M. Latypov, Y. Beygelzimer, and H. S. Kim, *Mater. Trans.* **54**, 1587 (2013).
31. M. I. Latypov, E. Y. Yoon, D. J. Lee, R. Kulagin, Y. Beygelzimer, M. Seyed Salehi, and H. S. Kim, *Metal. Mater. Trans*. **45A**, 2232 (2014).
32. S. Khoddam, A. Farhoumand, and P. Hodgson, *Mech. Mater.* **43**, 684 (2011).
33. J. Alkorta and J. Gil Sevillano, *J. Mater. Proc. Tech.* **141**, 313 (2003).
34. F. Silva, N. Medeiros, L. Moreira, J. Lins, and J. Gouvêa, *Mater. Sci. Eng. A* **546**, 180 (2012).
35. R. Kocich, J. Fiala, I. Szurman, A. Macháčková, and M. Mihola, *J. Mater. Sci.* **46**, 7865 (2011).